crystals

MDPI

Article

Effect of Al-Ti-B-Er on the Microstructure and Properties of Ultrahigh-Strength Aluminum Alloy

Xiao Wang [1], Zizhi Ying [1], En Hu [1], Juntao Ma [1], Xiaoqing Zhang [1], Tengfei Ma [2,*] and Xiaohong Wang [2,*]

[1] Zhejiang Weihong Metal Products Co., Ltd., Quzhou 324000, China
[2] Key Laboratory of Air-Driven Equipment Technology of Zhejiang Province, Quzhou University, Quzhou 324000, China
* Correspondence: 36105@qzc.edu.cn (T.M.); 36098@qzc.edu.cn (X.W.); Tel.: +86-571-8026716 (T.M.)

Abstract: To refine the grain size and improve the mechanical properties of ultrahigh-strength aluminum alloy (Al-10Zn-1.9Mg-1.6Cu-0.12Zr), the Al-Ti-B-Er grain refiner was prepared by the melt reaction method using the aluminum melt and Al + Ti + B precursor. The results exhibit that the Al-Ti-B-Er grain refiner is mainly composed of a block $TiAl_3$ phase, and loose agglomerated nano-sized TiB_2 and Al_3Er phases. The microstructure of ultrahigh-strength aluminum is significantly affected by the Al-Ti-B-Er refiner, which changes from dendrite to equiaxial grain with increasing Al-Ti-B-Er content, and the size of the eutectic phase is significantly refined. The high-efficiency refinement of Al-Ti-B-Er is due to Er promoting the uniform distribution of $TiAl_3$ particles and the formation of loose agglomerated nano-sized TiB_2 particles. The optimal addition content of Al-Ti-B-Er into ultrahigh-strength aluminum alloys is 1 wt%, whose grain size is approximately 40 μm. Additionally, the strength and ductility of ultrahigh-strength aluminum alloys are simultaneously improved by adding 1wt% Al-Ti-B-Er after the T6 treatment, reaching 756 MPa and 20%, respectively. This enhancement in strength and ductility is mainly attributed to grain refinement and the eutectic phase refinement.

Keywords: aluminum alloy; Al-Ti-B; grain refinement; mechanical property

check for updates

Citation: Wang, X.; Ying, Z.; Hu, E.; Ma, J.; Zhang, X.; Ma, T.; Wang, X. Effect of Al-Ti-B-Er on the Microstructure and Properties of Ultrahigh-Strength Aluminum Alloy. *Crystals* **2024**, *14*, 695. https://doi.org/10.3390/cryst14080695

Academic Editor: Umberto Prisco

Received: 1 July 2024
Revised: 23 July 2024
Accepted: 24 July 2024
Published: 30 July 2024

Copyright: © 2024 by the authors. Licensee MDPI, Basel, Switzerland. This article is an open access article distributed under the terms and conditions of the Creative Commons Attribution (CC BY) license (https://creativecommons.org/licenses/by/4.0/).

1. Introduction

High-strength aluminum alloys are mainly composed of Al-Zn-Mg-Cu series alloys, which are widely used in aircraft and rocket components [1–3]. High-strength aluminum alloys play an important role in both military and civilian aircraft [2]. From Boeing 727 to Boeing 767, the most successful uses are as follows: 7150-T651X is used for the upper airfoil, 2324-T39 and 2224-T3511 are the best lower airfoils, and 7075 alloy is used for thick forgings [4,5]. With the development of the aviation industry, the new generation of aircraft has put forward higher requirements for materials, such as light weight, high strength, high toughness, and corrosion resistance. The development of ultrahigh-strength aluminum alloys is basically focused on high strength and low toughness; high strength and high toughness; and high strength, high toughness and corrosion resistance. The subsequent development of heat treatment also follows in the direction of T6-T73-T76-T736 (T74)-T77 [6,7]. In terms of alloy designation, the alloying degree and the main alloying elements are becoming increasingly rationalized, and impurities such as Fe and Si are decreasing. Moreover, the addition of trace transition elements is becoming increasingly extensive. Then, the alloy shows excellent comprehensive properties, rather than increasing the strength and ductility [8,9].

Grain refiners are common additives in aluminum alloys and mainly play a role in grain refinement [10,11]. The grain refinement effect is an important indicator for evaluating the performance of a grain refiner, which is the most direct and reliable method. The refinement effect of a grain refiner is determined by factors such as the size, morphology,

and distribution of the particles in the grain refiner. Furthermore, the cooling rate during the refinement process is also important for the grain refinement effect. Rare earth elements are active substances that can improve the morphology of particles and are excellent modifiers. In recent years, Al-Ti-B-Re and Al-Ti-C-Re grain refiners have been developed by taking advantage of the metamorphic nature of rare earths to improve the morphology and distribution of particles in the grain refiner [12,13]. Consequently, the grain-refining efficiency of grain refiner is increased. In terms of grain-refining efficiency, the rare earth elements, Al-Ti-B and Al-Ti-C, can refine the grain size, and the composite grain refiner will be more efficient. An addition of the rare earth elements Ce and La into the grain refiner can hinder the growth of the $TiAl_3$ phase and reduce the size of $TiAl_3$, inhibiting the formation of needle-like $TiAl_3$ and improving the distribution of the $TiAl_3$ phase [14,15]. In the Al-Ti-B-Re grain refiner, TiB_2 is granular and has loose agglomerates that are homogenously distributed. When it is added to the aluminum melt, the rare earth elements are released and the wettability between borides and the molten aluminum is improved, then the movement of TiB_2 particles is inhabited and the growth and aggregation of TiB2 particles in the melt are avoided. Thus, precipitation and aggregation existing in a homogeneous state are not easily achieved, extending the effective action time [16,17]. It can be concluded that the highly efficient refinement results from more active TiB2 particles. Al-Ti-C-Re is more efficient than Al-Ti-C according to the grain refinement experiment. It reveals that rare earth elements improve the wettability of C in aluminum melts, promoting the formation of TiC [18]. The morphology of $TiAl_3$ particles is changed, and the grain size of pure Al is decreased from 350 μm to 50 μm after the addition of 0.5 wt% Al-Ti-C-Re. However, the grain refiner is mainly synthesized using the fluoride reaction method, resulting in low purity and high contamination. This method deteriorates the grain refiner and thus its applications in the aerospace field [19,20].

To improve the microstructure and properties of ultrahigh-strength aluminum alloy, the Al-10Zn-1.9Mg-1.6Cu-0.12Zr alloy is designed. Additionally, the highly efficient Al-5Ti-1B-Er grain refiner is synthesized using the melt reaction method with high purity. The effect of the Al-Ti-B-Er grain refiner on the microstructure and properties of ultrahigh-strength aluminum alloys was studied, and a corresponding mechanism is revealed.

2. Experimental Section

The Al-Ti-B-Er grain refiner is mainly prepared by the melt reaction method. The initial materials are Al power, Ti power and B power, which are homogeneously mixed using a ball-milling machine. Then, the mixed powder is compressed in an iron mold with a size of Φ50 mm × 20 mm. The aluminum ingot was heated to 780–800 °C in a resistance furnace, which was covered with a layer of cryolite-covering agent after the aluminum ingot completely melted. The Al-Er master alloy was pressed into the melt until the master alloy was completely melted and diffused uniformly. Then, the melt was heated to 800~900 °C, the mixed powder compact was pressed into the melt using a graphite bell jar, and the graphite rod was mechanically stirred, accelerating the reaction and alloy homogeneity. The reaction was sustained for 10 min. Then, the melt was subjected to flotation refining (C_2Cl_6) and stirred until the reaction was complete. After refining, the melt was allowed to stand for 5 min, and the temperature was measured by a K-type thermocouple. The slag was removed after the temperature decreased to 720 °C, and the melt was cast into an iron mold (preheated at 250 °C for 1 h). A stable casting rate was necessary to avoid insufficient pouring and flow breaks, and then the Al-Ti-B-Er grain refiner was obtained.

The high-strength aluminum alloy with a nominal chemical composition of Al-10 Zn-1.9Mg-1.6Cu-0.12Zr was designed, which was melted in a graphite crucible using resistance furnace heating. The nominal and actual chemical composition of a high-strength aluminum alloy was listed in Table 1. The initial materials were aluminum ingots (99.9%), zinc ingots (99.9%), magnesium ingots (99.9%), Al-4Zr master alloy, and Al-50Cu master alloy. The initial materials were melted in a graphite crucible and cast into a φ 90 × 100 mm

iron mold. Then, the ingot was cut using a band saw for the grain refinement test. The high-strength aluminum alloy was remelted at 750 °C in a resistance furnace and then the Al-Ti-B-Er grain refiner was added with different contents. After refining and slag removal, the melt was cast into an iron mold (preheated at 250 °C for 1 h). The high-strength aluminum alloy was subjected to dual-stage homogenization treatment at 400 °C × 4 h + 470 °C × 30 h. Then, the ingot was flayed to φ88 mm, and the sheet with a cross-sectional area of 6 × 50 mm^2 was extruded at 430 °C. The extruded speed was 5~8 mm/s.

Table 1. Chemical composition of ultrahigh-strength aluminum alloy (wt%).

	Zn	Mg	Cu	Zr	Al
Nominal composition	10	1.9	1.6	0.12	Bal
Actual composition	10.2	1.78	1.72	0.14	Bal

Chemical composition analysis was carried out on the inductively coupled plasma emission spectrometer (ICP) on an IRIS Advantage spectrometer (Thermo Jarrell Ash, Franklin, MA, USA) in the Beijing General Research Institute of Non-Ferrous Metals. A total of 50 g of powder was prepared for each sample for ICP analysis. The phase analysis of the Al-Ti-B-Er grain refiner and high-strength aluminum alloy was analyzed with an X-ray diffractometer (XRD, D/MAX-3C, Rigaku, Tokyo, Japan). The scanning degree was 20–90° with a scanning speed of 5°/min using Cu Kα. The Al-Ti-B-Er grain refiner and high-strength aluminum alloy were observed using metallographic microscopy (OM, IE500M, Guangzhou, China) and scanning electron microscopy (SEM, FEI Quanta 250, Hillsboro, OR, USA) with an energy-dispersive spectrometer (EDAX). The samples were mechanically ground using 400#, 800#, 1000#, 1500#, and 2000# water sandpaper including SiC abrasive grains; the properties of water sandpaper met the criteria of GB/T9258-2000, then were mechanically polished and chemical etched using Keller's reagent (1.5% HCl + 2.5% HNO_3 + 1.0% HF + 95% H_2O). The grain size was observed in OM and calculated using the metallographic method. Typically, the OM samples were cut from 1/2 radius of the ingot along the axial direction, and the grain size was determined by the cross-sectional size of dendrite branches, including lateral branches. The particles in the Al-Ti-B-Er grain refiner and eutectic phase in high-strength aluminum alloy were observed via SEM and analyzed via EDAX.

The extruded sheet was subjected to T6 heat treatment and then subjected to tensile testing. The tension test was performed on an MTS testing machine under a tension rate of 0.5 mm/min. The flat specimens with a size of 175 × 25 × 6.5 mm^3 (length × width × thickness) were standard plate-shaped specimens. The tensile fracture was observed using SEM and the corresponding fracture mechanism was revealed.

3. Results and Discussion

The phase analysis of the Al-Ti-B-Er grain refiner was performed by XRD, as shown in Figure 1. The Al-Ti-B-Er grain refiner is mainly composed of $TiAl_3$ (PDF#49-1446) and TiB2 (PDF#35-0741) phases. Studies have shown that the addition of Er into aluminum alloys can form the Al_3Er phase. However, due to the low content of Er element in this experiment (0.1 wt%), it could not be analyzed by XRD.

In Figure 2, it can be seen that there are blocky particles and aggregated particles in the Al-Ti-B-Er refiner. The results show that the alloy is mainly composed of massive phases, bright white phases, and cluster-like phases. After the addition of rare earth elements, blocky particles and aggregated particles are distributed relatively uniformly. The size of massive block particles is about 10–20 μm, which is considered to be the $TiAl_3$ phase. The loose clumps are regarded as the aggregation of TiB_2. Rare earth elements improve the wettability of B and Ti powder in the aluminum melt, promoting the reaction. The solid solubility of Er in aluminum is low (at room temperature, the solubility of Er in aluminum or aluminum alloy is less than 0.046 at%), which exists in a free state [21]. At the same

time, the Er element is a surface-active substance, which is easy to adsorb on the grain boundary and phase interface, hindering the growth of $TiAl_3$ particles and reducing the size of $TiAl_3$, as well as inhibiting the formation of needle strip $TiAl_3$. The Er element makes it difficult for TiB_2 to aggregate and precipitate in the melt, resulting in the formation of fine and dispersed TiB_2 particles. Thus, the aggregation tendency of TiB_2 during refinement is reduced, increasing the number of heterogeneous nucleated cores.

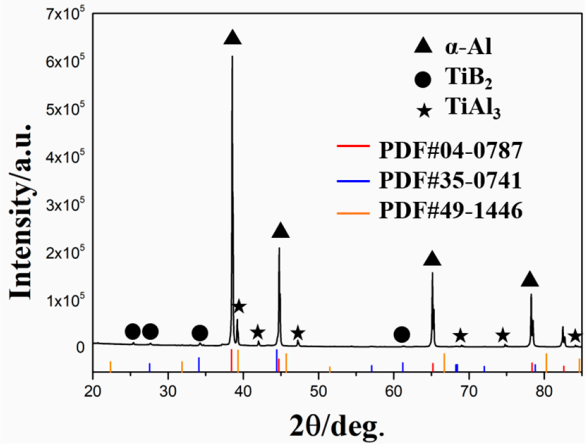

Figure 1. XRD patterns of the Al-Ti-B-Er grain refiner.

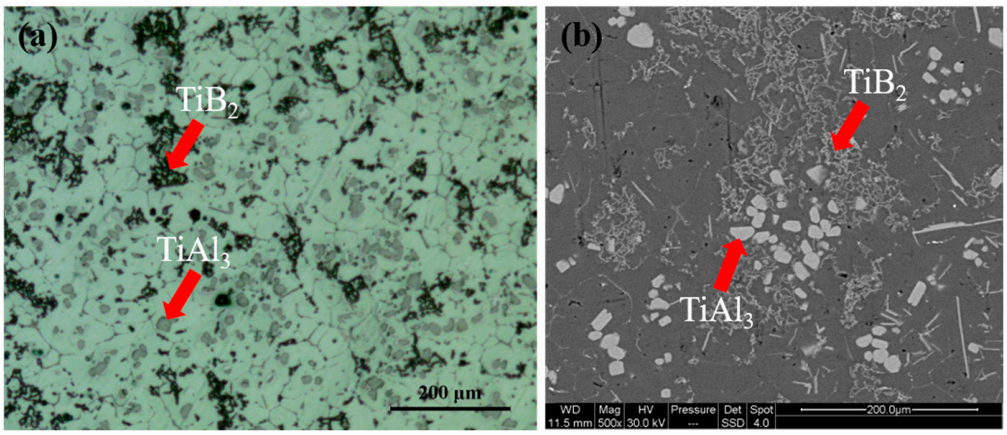

Figure 2. The initial microstructure of the Al-Ti-B-Er grain refiner: (**a**) OM image and (**b**) SEM image.

The Al-Ti-B-Er grain refiner was studied (Figure 3) carefully, including the morphology, size and distribution characteristics of the particles. The chemical elemental composition of the different phases was analyzed using EDS, as shown in Figure 3b–d. The white particles or aggregates referred to by A and C were enriched in Er element and identified as the AlEr phase by energy spectrometry. Al_3Er is commonly seen in addition to Er in aluminum alloys, and the bright white is determined to be the Al_3Er phase according to the stoichiometric ratio [22]. The massive phases with sizes of 10–20 μm were marked as B, composed of Ti and Al elements and determined to be the $TiAl_3$ phase based on the stoichiometric ratio. The contrast of cluster-like phases is close to the matrix, and the particles are inferred to be the TiB2 phase according to the XRD results.

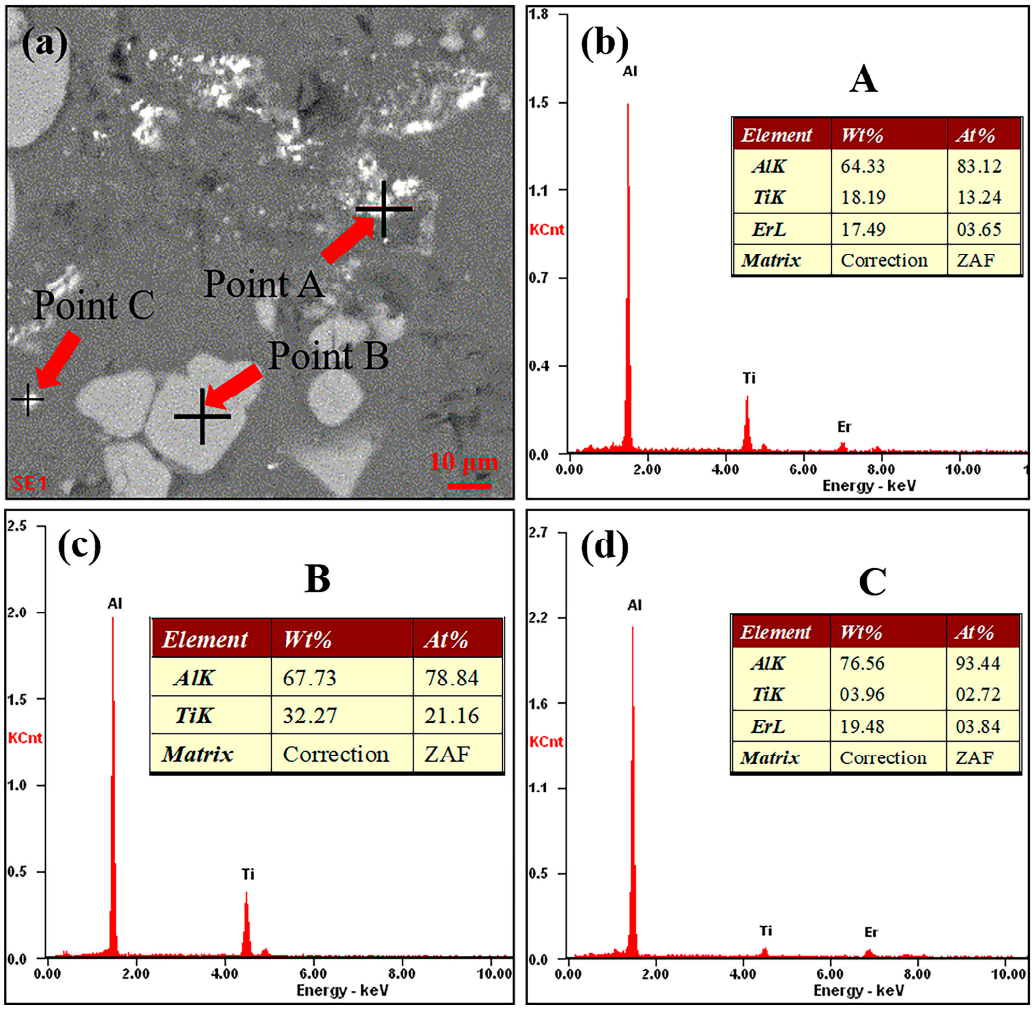

Figure 3. Semiquantitative analysis of Al-Ti-B-Er grain refiner: (**a**) partial SEM image, (**b**) point A analysis, (**c**) point B analysis, and (**d**) point C analysis.

The optimal addition amount of the Al-Ti-B-Er grain refiner in ultrahigh-strength aluminum alloys is determined and the effect of the Al-Ti-B-Er grain refiner on the microstructural evolution is revealed, such as the initial eutectic phase and grain size (this corresponds to the cross-sectional size of dendrite branches, including lateral branches). The microstructure of Al-10Zn-1.9Mg-1.6Cu-0.12Zr shows a typical dendritic structure with a grain size of approximately 300 μm, as shown in Figure 4a. Microstructures after adding different contents of Al-Ti-B-Er are shown in Figure 4b–f; the results show that the grain size gradually decreases with the increase in Al-Ti-B-Er contents. The grain size reached the minimum of 40 μm after an addition of 1wt% Al-Ti-B-Er. However, the grain size is not refined, and requires the addition of more grain refiner, denoting that 1wt% is the optimum addition content for the ultrahigh-strength aluminum alloys. In addition, the dendrites morphology changed significantly from dendrites to equiaxed grains. The grain refiner is hereditary, and the initial microstructure of the refiner is helpful for improving the refinement efficiency. The $TiAl_3$, TiB_2, and AlEr particles are released after the addition of Al-Ti-B-Er into the aluminum melt. Studies have shown that there is excellent coherence between $TiAl_3$, TiB_2 and α-Al, which is good for heterogeneous nucleation sites. In Al-Ti-B-Er, TiAl3 shows block morphology with a size of approximately 30 μm, and TiB_2 in the agglomerated group has a size of 1~2 μm [23,24]. When $TiAl_3$ and TiB_2 are large in quantity and homogenously distributed, then the number of effective heterogeneous nucleation sites is increased, resulting in highly efficient refinement.

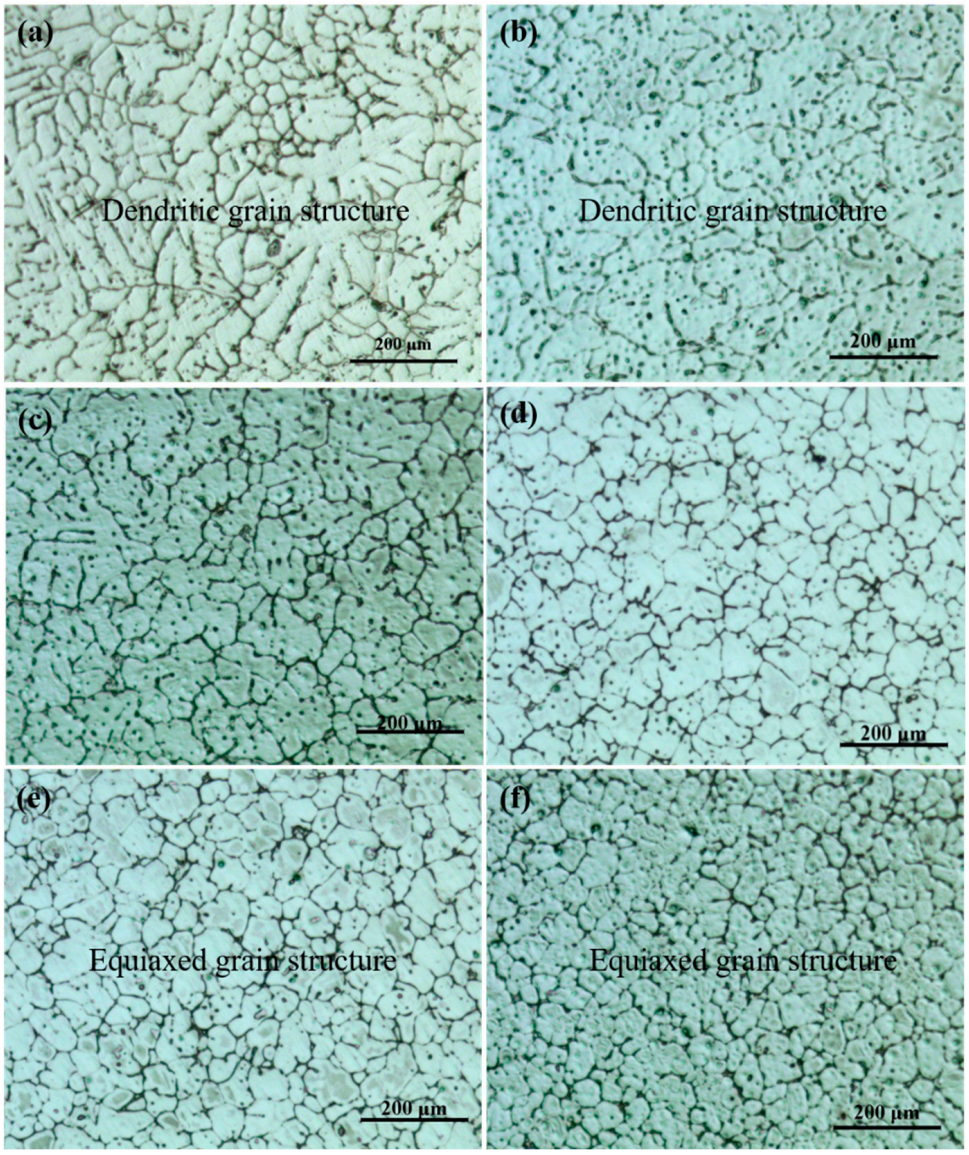

Figure 4. Effect of Al-Ti-B-Er on the microstructure of ultrahigh-strength aluminum alloys: (**a**) 0, (**b**) 0.2, (**c**) 0.5, (**d**) 0.7, (**e**) 1.0, and (**f**) 2.0.

With increasing alloying element content, the segregation becomes more serious during the solidification process. Cu and Zn elements are considered to segregate at dendrites and grain boundaries, forming a large component undercooling at the front of the solid–liquid interface and making the solid–liquid interface unstable. Grain growth stops when dendrites collide, and dendrite coarsening and secondary dendrite growth occurs. The solute aggregates at the interdendritic zone and reaches the eutectic composition point, where the eutectic reaction occurs and eutectic phases, such as $MgZn_2$ and AlZnMgCu, are formed [25,26]. The Al-10Zn-1.9Mg-1.6Cu-0.12Zr alloy shows a coarse eutectic structure. However, the eutectic phase is significantly refined after the addition of 1 wt% Al-Ti-B-Er, and its distribution is uniform. It is revealed that the skeletal morphology and spherical morphology of eutectic phases are mainly the $MgZn_2$ and AlZnMgCu phases, as shown in Figure 5c. The grain size is significantly decreased and the number of grain boundaries is increased after the addition of Al-Ti-B-Er, resulting in the alloying elements being able to distribute at more grain boundaries, thereby refining the eutectic phase. At the same time, the small grain size decreases the movement distance of the solid–liquid interface as well

as alloying elements, leading to a relative increase in the solidification rate. Consequently, more alloying elements are dissolved in the matrix, reducing the interdendritic segregation.

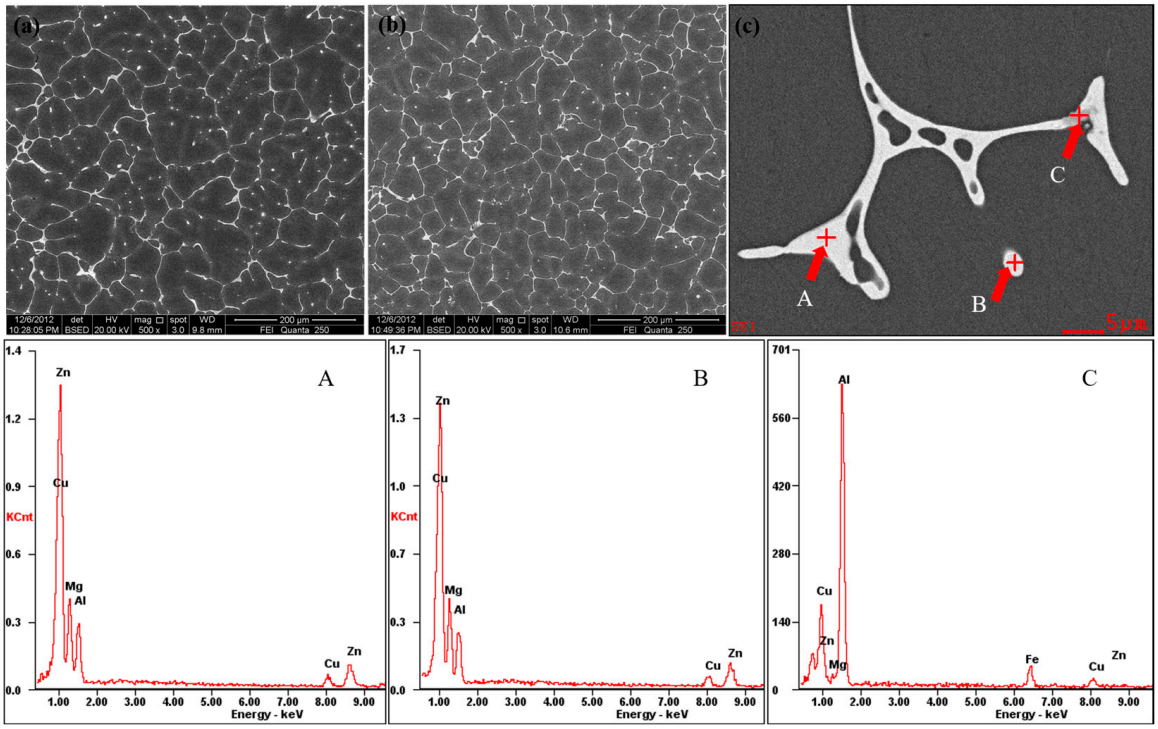

Figure 5. SEM morphology and EDS analysis of the ultrahigh-strength aluminum alloy: (**a**) 0 Al-Ti-B-0.1Er, (**b**) addition of 1 wt% Al-Ti-B-0.1Er, and (**c**) EDS analysis.

The existing forms of TiB_2, $MgZn_2$ and Al_3Zr particles in the ultrahigh-strength aluminum alloys were performed using TEM. As shown in Figure 6, black spherical particles are observed, which can be determined to be Al_3Zr particles according to the selected area electron diffraction (SAED) results. They are mainly distributed in the matrix to refine the grains and improve the mechanical property. The refinement mechanism of zirconium-induced aluminum alloys varies with the change in zirconium content. When the Zr content is low, the interactions between Zr and the clustered atomic groups form stable atomic groups, which eventually develop into crystal nuclei. However, α-Al nucleates through the peritectic reaction as the Zr content is high [27]. It has been observed that the refinement of Al_3Zr particles is mainly attributed to heterogeneous nucleation. Al3Zr shows two typical crystal structures, one of which is the L12 type, and the mismatch degree with α-Al is 0.75%. One is the Do22-type, whose mismatch degree with α-Al is 2.89%. Better coherence between the second particles and the matrix helps to lower the interfacial free energy of the system. Then, Al3Zr is an effective heterogeneous nucleation core due to good coherence with the α-Al matrix. The TiB_2 particles are observed in the high-strength aluminum alloy, indicating that the TiB_2 particles also act as a heterogeneous nucleation core, as shown in Figure 6b. TiB_2 and α-Al are coherent, and there are two pairs of coherent surfaces, $<110>Al \| <11\bar{2}0>TiB_2$ and $<110>Al \| <10\bar{1}0>TiB_2$, which are good heterogeneous nucleation cores. TiB_2 and Al_3Zr are both effective heterogeneous nucleation cores that can refine ultrahigh-strength aluminum alloys. At the same time, a lath-shaped η-phase is also observed, which is the main strengthening phase.

The ultrahigh-strength aluminum alloy was subjected to hot extrusion forming, followed by T6 treatment. After the addition of Al-Ti-B-Er grain refiner, the strength and ductility of the ultrahigh-strength aluminum are improved simultaneously, as shown in Figure 7. The synergistic improvement in strength ductility after the addition of 1 wt% Al-Ti-B-Er grain refiner is mainly due to the grain refinement as well as the refinement

of the eutectic phase, which also causes the uniform distribution of the eutectic phase. Grain refinement and eutectic phase refinement are conducive to the dissolution of the eutectic phase during the homogenization process, thereby improving the solid solubility of alloying elements and promoting the precipitation of the strengthening phase during the aging process [28]. Then, the mechanical properties can be improved reasonably. In addition, the eutectic phase in the alloy involves a hard and brittle phase, which is the main source of crack initiation. The grain refiner-induced refinement effect on the eutectic phase improves the ductility of the alloy.

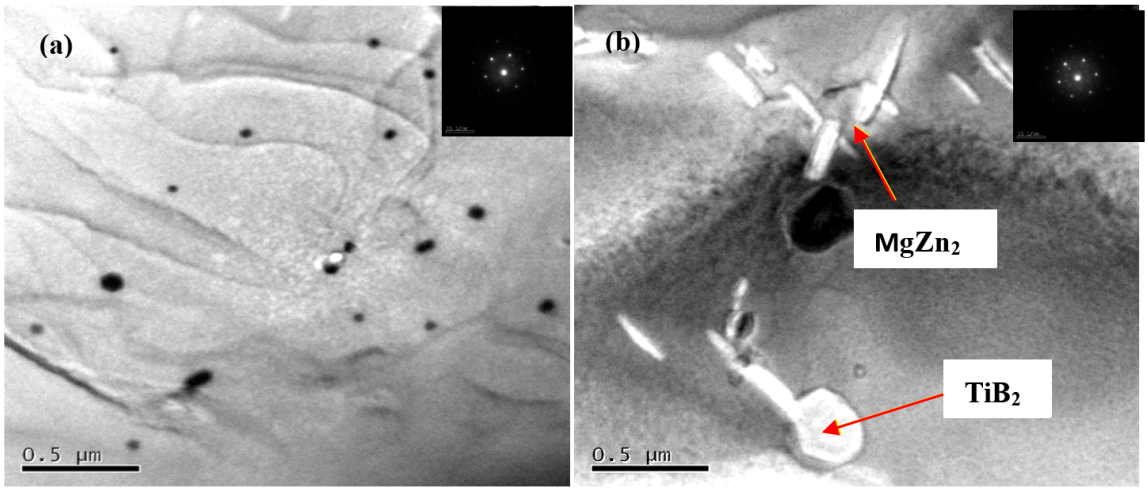

Figure 6. TEM images of the ultrahigh-strength aluminum alloy: (**a**) Al_3Zr particles, (**b**) TiB_2 particles and $MgZn_2$ particles.

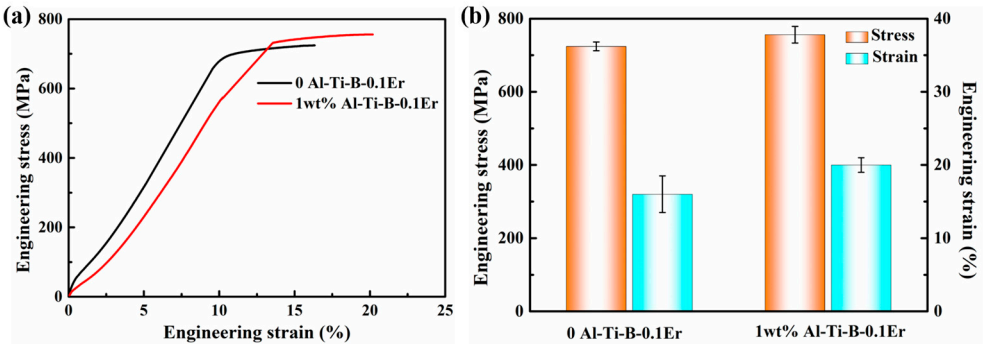

Figure 7. Tensile property of the ultrahigh-strength aluminum alloy: (**a**) engineering stress–strain curves; (**b**) corresponding ultimate tensile strength and fracture strain.

The tensile fracture morphology of the ultrahigh-strength aluminum alloy at room temperature is shown in Figure 8. Without the addition of the Al-Ti-B-Er grain refiner, the fracture exhibits a cleavage fracture mode. Small and shallow dimples are observed under high magnification. This fracture mode is a brittle fracture caused by the second particles, as shown in Figure 8a,b. After the addition of the Al-Ti-B-Er grain refiner, the fracture also maintains a cleavage fracture mode. However, the size of the dimples is larger compared to that without the addition of Al-Ti-B-Er under the high magnification. Moreover, they are relatively shallow, indicating a brittle fracture (Figure 8c,d). In ultrahigh-strength aluminum alloys, second particles are the main source of crack initiation and propagation by tearing. The second particles hinder the crack propagation, which is beneficial for improving ductility. The addition of the Al-Ti-B-Er grain refiner helps to improve ductility, which is mainly attributed to the multiscale second particles in Al-Ti-B-Er impeding the crack propagation and improving ductility, displaying a small increase in elongation [23].

However, the addition of the Al-Ti-B-Er grain refiner does not change the fracture mode of ultrahigh-strength aluminum alloys, which is still a brittle fracture.

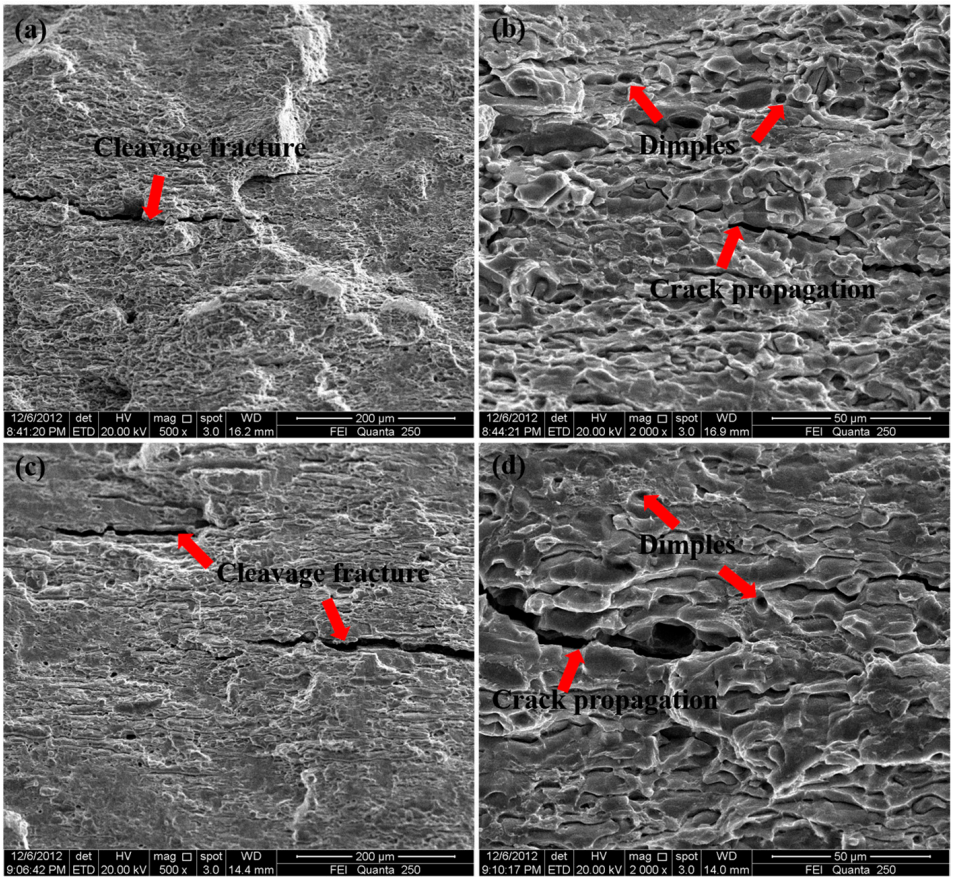

Figure 8. Fracture morphology of the ultrahigh-strength aluminum alloy: (**a**) 0 Al-Ti-B-Er, (**b**) high-magnification morphology, (**c**) addition of 1% Al-Ti-B-Er, and (**d**) high-magnification morphology.

4. Conclusions

The Al-Ti-B-Er grain refiner was prepared by the melt reaction method, and was applied to the Al-10Zn-1.9Mg-1.6Cu-0.12Zr ultrahigh-strength aluminum. The effect of Al-Ti-B-Er grain refiner on the microstructure and properties of ultrahigh-strength aluminum alloys was studied, and the conclusions are summarized as follows:

1. The Al-Ti-B-Er grain refiner is mainly composed of the block $TiAl_3$ phase with a size of 10–20 μm, and loose agglomerated nano-sized TiB_2 and Al_3Er phases. Notably, nanoscale TiB_2 and Al_3Er particles exhibit excellent refinement ability in ultrahigh-strength aluminum.
2. The microstructure of ultrahigh-strength aluminum changes from dendrite to equiaxial grain with increasing Al-Ti-B-Er content, and the size of the eutectic phase is significantly refined. Er promoted the uniform distribution of $TiAl_3$ particles and the formation of loose agglomerated nano-sized TiB_2 particles. Typically, the grain size is reduced from ~300 μm to approximately 40 μm by adding 1 wt% Al-Ti-B-Er into ultrahigh-strength aluminum alloys.
3. After T6 treatment, the tensile results reveal that the ultrahigh-strength aluminum alloy exhibits superior strength and ductility (756 MPa/20%) with adding 1 wt% Al-Ti-B-Er. This enhancement in strength and ductility is attributed to the refinement of grain and the eutectic phase.
4. The Al-Ti-B-Er grain refiner displays a grain refinement limitation of approximately 40 μm in ultrahigh-strength aluminum. It may be an effective way by adding various

rare elements to the grain refiner to push the grain refinement limitation and further improve the mechanical properties of ultrahigh-strength aluminum.

Author Contributions: Conceptualization, T.M. and X.W. (Xiaohong Wang); writing—original draft preparation, X.W. (Xiao Wang) and Z.Y.; methodology, E.H.; software, J.M.; investigation, X.Z.; data curation X.W. (Xiao Wang) and Z.Y.; writing—review and editing T.M. and X.W. (Xiaohong Wang); funding acquisition, T.M. All authors have read and agreed to the published version of the manuscript.

Funding: This research was funded by the Zhejiang Province Natural Science Foundation of China, grant number LZY22E010001.

Data Availability Statement: The original contributions presented in the study are included in the article, further inquiries can be directed to the corresponding authors.

Conflicts of Interest: Authors Xiao Wang, Zizhi Ying, En Hu, Juntao Ma, Xiaoqing Zhang were employed by the company Zhejiang Weihong Metal Products Co., Ltd. The remaining authors declare that the research were conducted in the absence of any commercial or financial relationships that could be construed as a potential conflict of interest.

References

1. Lin, G.; Zheng, X.; Yang, W.; Feng, D.; Peng, D. Study on the hot deformation behavior of Al-Zn-Mg-Cu-Cr aluminum alloy during multi-stage hot compression. *Acta Metall. Sin.* **2009**, *22*, 110–116. [CrossRef]
2. Goel, P.; Khan, N.Z.; Khan, Z.A.; Ahmari, A.; Gangil, N.; Abidi, M.H.; Siddiquee, A.N. Investigation on material mixing during FSW of AA7475 to AISI304. *Mater. Manuf. Process.* **2019**, *34*, 192–200. [CrossRef]
3. Liu, X.; Liu, Y.; Zhou, Z.; Zhan, Q. Enhanced strength and ductility in Al-Zn-Mg-Cu alloys fabricated by laser powder bed fusion using a synergistic grain-refining strategy. *J. Mater. Sci. Technol.* **2022**, *124*, 12441–12452. [CrossRef]
4. Plies, J.B.; Grant, N. Structure and properties of spray formed 7150 containing Fe and Si. *Int. J. Powder Metall.* **1994**, *30*, 335–343.
5. Lukasak, D.A.; Hart, R.M. Aluminum alloy development efforts for compression dominated structure of aircraft. *Light Met. Age* **1991**, *49*, 11–15.
6. Zhang, W.; Xu, J. Advanced lightweight materials for Automobiles: A review. *Mater. Des.* **2022**, *221*, 110994. [CrossRef]
7. Yasir, M.K.; Rehan, U.; Ahmed, K.K. Review of recent trends and developments in aluminium 7075 alloy and its metal matrix composites (MMCs) for aircraft applications. *Results Eng.* **2023**, *20*, 101372.
8. Lei, Z.; Wen, S.; Huang, H.; Wei, W.; Nie, Z. Grain refinement of aluminum and aluminum alloys by Sc and Zr. *Metals* **2023**, *13*, 751. [CrossRef]
9. Yao, E.; Zhang, H.; Ma, K.; Ai, C.; Gao, Q.; Lin, X. Effect of deep cryogenic treatment on microstructures and performances of aluminum alloys: A review. *J. Mater. Res. Technol.* **2023**, *26*, 3661–3675. [CrossRef]
10. Liu, G.; Ren, Y.; Ma, W.; Morita, K.; Lei, Y.; Zhan, S.; Lv, G.; Li, S.; Zeng, Y.; Li, R. Development process and future trends of chemical refining agents' influence on grain refinement in aluminum alloys. *J. Mater. Res. Technol.* **2024**, *29*, 242–257. [CrossRef]
11. Zhao, C.; Li, Y.; Xu, J.; Luo, Q.; Jiang, Y.; Xiao, Q.; Li, Q. Enhanced grain refinement of Al-Si alloys by novel Al-VB refiners. *J. Mater. Sci. Technol.* **2021**, *94*, 104–120. [CrossRef]
12. Wang, X.-J.; Xu, C.; Muhammad, A.; Hanada, S.; Yamagata, H.; Wang, W.-H.; Ma, C.-L. Effects of Al-Ti-B-RE grain refiner on microstructure and mechanical properties of Al-7.0Si-0.55Mg alloy. *Trans. Nonferr. Met. Soc. China* **2014**, *24*, 2244–2250. [CrossRef]
13. Ding, W.; Zhao, X.; Taili, C.; Haixia, Z.; Liu, X.; Cheng, Y.; Lei, D. Effect of rare earth Y and AleTieB master alloy on the microstructure and mechanical properties of 6063 aluminum alloy. *J. Alloys Compd.* **2020**, *830*, 154685. [CrossRef]
14. Meng, C.; Tang, H.; Wang, C.; Sun, Y.; Peng, F.; Zheng, X.; Wang, J. Anti-fading study of Al–Ti–B by adding Ce on 6111 aluminum alloy. *J. Mater. Res. Technol.* **2024**, *30*, 2420–2434. [CrossRef]
15. Lili, S.; Gaosheng, F.; Longze, L.; Hongling, C.; Huosheng, W. Effect of Ce in Al-Ti-B-Ce refiner on TiAl3/α-Al heterogeneous nucleation interface by first-principles study. *J. Mater. Eng. Perform.* **2023**, *32*, 8585–8592. [CrossRef]
16. Yin, D.-S.; Zhang, N.; Chen, K.-J.; Zhang, Y.-L. Effect of Gd on microstructure and refinement performance of Al-5Ti-B alloy. *China Foundry* **2021**, *18*, 223–228. [CrossRef]
17. Wang, J.Z. Research on a new type grain refiner refining α-al by adding molten state and diluted Al-Ti-B-RE master alloy. *Adv. Mater. Res.* **2012**, *535–537*, 915–918. [CrossRef]
18. Zhao, H.; Song, Y.; Li, M.; Guan, S. Grain refining efficiency and microstructure of Al–Ti–C–RE master alloy. *J. Alloys Compd.* **2010**, *508*, 206–211. [CrossRef]
19. Whitebead, J.A.; Danilak, S.A. The development of a commercial Al-3% Ti-0. 05% C grain refining master alloy. *Lightmetals* **1997**, 77–84.
20. Wang, L.D.; Zhu, D.Y.; Wei, Z.L.; Huang, L.G.; Song, W.; Chen, Y.L. The refinement effect of Al-Ti-C-RE master alloy prepared by adding Cesub2/subOsub3/sub on pure Al. *Adv. Mater. Res.* **2010**, *139*, 227–234.
21. Okamoto, H. Al-Er (Aluminum-Erbium). *J. Phase Equilibria Diffus.* **2011**, *32*, 261–262. [CrossRef]

22. Xu, L.; Lv, J.; Tang, H.; Huang, D. Phase equilibria and solidification characteristics in the Al-rich region of the Al-Ti-Er system. *J. Alloys Compd.* **2024**, *980*, 173667. [CrossRef]
23. Furuta, S.; Minagawa, A.; Murakami, Y.; Omura, N.; Akihisa, T.; Masayuki, U.; Kobayashi, M. Heterogeneous nucleation behavior of solidified α-Al phase on agglomerated TiB2 particles in aluminum-copper alloy: Study by synchrotron radiation multiscale tomography. *Materialia* **2023**, *28*, 101763. [CrossRef]
24. Ma, T.; Chen, Z.; Nie, Z.; Huang, H. Microstructure of Al-Ti-B-Er refiner and its grain refining performance. *J. Rare Earths* **2013**, *31*, 622–627. [CrossRef]
25. Hadjadj, L.; Amira, R. The effect of Cu addition on the precipitation and redissolution in Al–Zn–Mg alloy by the differential dilatometry. *J. Alloys Compd.* **2009**, *484*, 891–895. [CrossRef]
26. Li, Y.; Wang, Y.; Lu, B.; Yu, W.; Wang, H.; Xu, G.; Wang, Z. Effects of Cu content on the precipitation process of Al-Zn-Mg alloys. *J. Mater. Sci.* **2012**, *47*, 8174–8187.
27. Knipling, E.K.; Dunand, C.D.; Seidman, N.D. Precipitation evolution in Al-Zr and Al-Zr-Ti alloys during isothermal aging at 375–425 deg. *Acta Mater.* **2008**, *56*, 114–127. [CrossRef]
28. Wen, K.; Li, X.-W.; Xiong, B.-Q.; Liu, H.-L.; Wang, Y.-J.; Li, Z.-H.; Zhang, Y.-A.; Li, Y.-N. Influence of minor Sc additions on grain refinement and microstructure characteristics of a high Zn-containing Al-Zn-Mg-Cu-Zr alloy. *J. Cent. South Univ.* **2022**, *29*, 780–794. [CrossRef]

Disclaimer/Publisher's Note: The statements, opinions and data contained in all publications are solely those of the individual author(s) and contributor(s) and not of MDPI and/or the editor(s). MDPI and/or the editor(s) disclaim responsibility for any injury to people or property resulting from any ideas, methods, instructions or products referred to in the content.